Implementation of a neuromorphic vestibular sensor with analog VLSI neurons

Giovanni Passetti*‡, Federico Corradi†‡, Marco Raglianti*‡, Davide Zambrano*‡, Cecilia Laschi*, and Giacomo Indiveri†
*The BioRobotics Institute, Scuola Superiore Sant'Anna, Pisa, Italia
Email {giovanni.passetti,marco.raglianti,d.zambrano,cecilia.laschi}@ssup.it
†Institute of Neuroinformatics, University of Zürich and ETH Zürich, Switzerland
Email: {federico,giacomo}@phys.ini.uzh.ch
‡All these authors have same contribution.

***Abstract*— This work aims at implementing an event driven neuromorphic vestibular sensor using a commercial Inertial Measurement Unit (IMU) and a custom analog VLSI neuromorphic chip. We investigate a model of the vestibular sensor that emulates the spiking responses of hair cells in the semicircular canals. We calibrate the neuromorphic chip to match the parameters of a neuroscientific computational model. Experimental results validating the hardware implementation and the calibration procedure are presented.**

I. Introduction

The vestibular system detects motion of the head relative to space and gravity, representing our reference frame for the movements and orientations in space [1], [2]. It is involved in several systems for maintaining both head and body posture, and it compensates for head movements in the visual axis in order to stabilize vision. In general, it plays a key role in the definition of our sense of movement [3]. Understanding the function of the vestibular system and implementing it in compact low-power electronic hardware can be extremely useful for both basic research investigations and practical applications (e.g. in the field of humanoid robotics or neuroprosthetics) [4].

The vestibular system is comprised of the two otholith organs, which detect linear accelerations, and the three semicircular canals, which detect angular velocities, over the frequency range of the natural movement (0–20 Hz). This work aims at developing a physical model of the vestibular system by emulating the functionalities of the semicircular canal afferents via biophysically realistic *neuromorphic* circuits. Neuromorphic engineering aims at reproducing the principles of neural computation implementing hardware (mainly electronic) systems that can efficiently interact with the environment in real-time thus contributing to the validation of the biological principle itself [5]. Moreover, a spiking vestibular sensor could be easily integrated in robotic applications based on low-power, highly parallel neuromorphic computational architectures.

This work shows an implementation of a neuromorphic vestibular sensor using a commercial Inertial Measurement Unit (IMU) and a custom analog VLSI neuromorphic chip. The following sections describe the main elements of the developed sensor and the results demonstrate the validity of the system with respect to the biological counterpart.

TABLE I

The model parameters: shared (a) and different (b) parameters of the regular and irregular afferents.

	Common
τ_v (ms)	1
τ_w (ms)	9.5
w_0	0.05
T_{refrac} (ms)	1
τ_a (ms)	20

(a)

	Regular	Irregular
I_{bias}	0.0515	0.049
Δw	0.003	0.001
σ	0.00007	0.0015
G_H (ms/deg)	0.0156	0.0315
G_A (ms/deg)	0	0.0315

(b)

II. Materials and Methods

A. The model

We investigate a model of the vestibular sensor that emulates the spike timing response of the hair cells present in the semicircular canals. A detailed analysis of the thousands of afferents coming form this apparatus is out of the scope of this work, thus only a few afferents will be emulated. However, in order to fully characterize the information carried out by the vestibular afferents, the different features of the cells involved will be considered. Afferents in this system are characterized as either regular or irregular on the basis of their resting discharge, which is correlated to distinct morphological features at their peripheral terminations [1], [2]. Sadeghi et al. (2007) showed the role of variability into information transmission, suggesting that the two neuronal populations coexist in the peripheral sensory system. The information carried on by the regular afferents are related to the precise timing of action potentials (temporal code), while the irregular afferents can be associated with rate code. As a consequence, irregular afferents best encode information for high frequencies (as suggested in [6]) whereas regular afferents transmit information about the detailed time course of the stimulus.

The neuron model used in our analysis of the vestibular afferents is a modified leaky integrate-and-fire neuron with a dynamic threshold [1]. We briefly report the fundamental model equations in order to introduce the parameters used to

978-1-4799-1471-5/13/$31.00 ©2013 IEEE

calibrate the response of the silicon neuron chip. The hair cells of the receptor organs mainly respond to a predefined orientation. At resting state, these cells are active with a resting discharge with low rate of variability for the regular cells and high rate of variability for the irregular ones. A deflection in the preferred direction causes depolarization of the membrane potential (the firing rate increases) and a deflection in the opposite direction causes its hyperpolarization (the firing rate decreases). The afferent cells coming from the three canals encode head velocities in the three mutually orthogonal axes. We did not take into account the individualized biomechanics and sensitivity to inertia of biological hair cells but, due to the mismatch in integrated circuits fabrication, significant variability can be obtained by connecting the same transducer to different silicon afferent neurons.

The membrane voltage v and threshold w, over times between action potentials, obey the following differential equations (note that the model emulates only the spike timing response and that voltages and currents are dimensionless):

$$\dot{v} = -\frac{v}{\tau_v} + \frac{I_{\text{synap}}}{\tau_v} \tag{1}$$

$$\dot{w} = (w_0 - w)/\tau_w \tag{2}$$

where τ_v is the membrane time constant, τ_w is the threshold recovery time constant, and w_0 is the equilibrium value for the threshold. When $v(t) = w(t)$ an action potential is produced, and w is incremented by Δw, while v is reset and forced to 0 for T_{refrac} ms. The resulting threshold is therefore self adapting to repetitive firing by hyper-polarization, with an upper bound dependent on T_{refrac}.

The synaptic current I_{synap} is:

$$I_{\text{synap}} = G_H HV(t) - G_A X_A(t) + I_{\text{bias}} + \sigma\xi(t) \tag{3}$$

$$\dot{X}_A = -\frac{X_A}{\tau_A} + \frac{HV(t)}{\tau_A} \tag{4}$$

where $HV(t)$ is the head rotational velocity with respect to the considered axis, I_{bias} is a constant bias current, $\sigma\xi$ is Gaussian white noise with zero mean and SD σ and G_H is the intensity of the signal. In case of irregular afferents the function $HV(t)$ is low-pass filtered (with cutoff frequency 50 Hz $= 1/\tau_a$) to obtain X_A, which is then subtracted with a gain G_A from $G_H HV(t)$. Table I shows the model parameters.

B. The sensor

To measure angular velocities around the three axes we used an iNEMO-M1 IMU, produced by STMicrolelectronics (STM). The device includes, besides other components, a Microelectromechanical 16-bit digital output gyroscope (L3GD20) and a 32-bit ARM microprocessor (STM32F103RE MCU). The ARM core runs a firmware written in C programming language, and compiled with the GNUARM toolchain.

The gyroscope has been set to sample angular velocities around the three axes at 10 ms time intervals (100 Hz), with full-scale input range $HV_{fs} = \pm 250$ deg/s and nominal sensitivity $8.75 \cdot 10^{-3}$ dps/digit. Acquired samples are digitally low-pass filtered with cutoff frequency set to 25 Hz, and made available to the MCU. Every 10 ms gyro's sampling procedure generates a *data ready event*. The sampled values are asynchronously read through the Serial Peripheral Interface. Three independent timer registers (one for each axis) are updated in order to produce, by hardware interrupts, a stable pulse density modulated (PDM) output on the iNEMO platform's general purpose I/O pins. Angular velocities are encoded as output pulses according to the Address Event Representation (AER) [7] using a two-bits address to identify the axis of each pulse.

The pulse frequency for each channel (f_c) is the linear interpolation of the gyroscope's output on the range of frequencies between $f_{\min} = 300$ Hz and $f_{\max} = 1500$ Hz (corresponding respectively to the highest negative and positive velocity):

$$f_c = \frac{f_{\max} - f_{\min}}{2|HV_{fs}|} HV_c + \frac{f_{\max} + f_{\min}}{2} \tag{5}$$

where c is either the x, y or z channel.

The 16-bit countdown register of the timer is set at $\texttt{round}(\text{TIM\_CLK}/f_c)$, with $\text{TIM\_CLK} = 18$ MHz, thus generating a *pulse event* at the desired frequency.

In conjunction with preemptive scheduling of the interrupt service routines, the timer has been set to a higher priority with respect to the gyroscope's reading in order to limit spurious variations in pulse frequencies.

C. The neuromorphic VLSI device

The neuromorphic device is a multi-neuron chip, fabricated using a standard $0.18\mu m$ Complementary Metal Oxide Semiconductor (CMOS) 1-poly 4-metal process. The chip contains 58 adaptive exponential integrate-and-fire-neurons [8], and 58×32 programmable synapses [9]. For the details of the implementation we refer to the neuron circuit described in [10].

The neuron circuit has been shown to be able to reproduce a wide range of spiking behaviors. The dynamics of the membrane potential is well described by a two variables system of differential equations [8]. One term represents the activation function (membrane voltage), with an exponential voltage dependence. This membrane voltage term is coupled to a second equation which describes the adapting behaviour of the neuron.

In this work, we matched the parameters of the proposed theoretical model with silicon neurons following a calibration procedure that is described below. Even though the theoretical model is not an exponential adaptive Integrate-and-Fire model (but just a pure linear one) we demonstrate experimentally how the dynamics of our silicon neuron successfully match the theoretical predictions.

In what follows we provide the results of the calibration process: the afferent neurons in the vestibular system, as stated in eqn. (3), receive different contributions that form the total synaptic current. The constant I_{bias} term is implemented with a direct constant current injected in the soma.

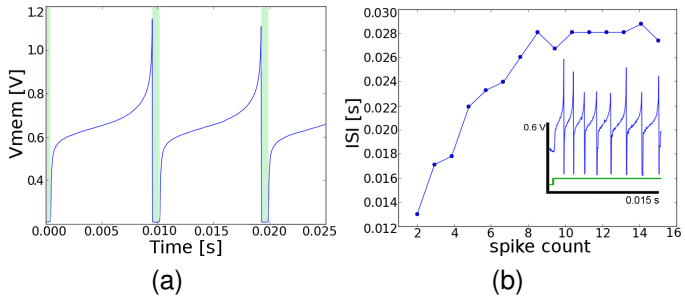

Fig. 1. **Neuron calibration** (a) neuron membrane potential. The shaded area shows the refractory period $T_{\text{refrac}} = 1$ ms. (b) Spike frequency adaptation. The neuron settles into an adapted state after about 7 spikes. The figure inset shows the membrane potential over time. The bottom trace in the inset represents the input current step.

1) Neuron soma parameters: have been configured to have a refractory period $T_{\text{refrac}} = 1$ ms (see Fig. 1a). The constant injected bias current (I_{bias}) has been calibrated such that the neuron at rest would fire at about 100 Hz (see Fig. 1).

2) Spike frequency adaptation: is an important feature of the model. The neuron's adaptation rate can be controlled by setting bias voltages that affect its time constant, equivalent to τ_w of eq. (2), and its amplitude (see also circuit description in [10]). In Fig. 1b we show how the spike frequency adaptation was calibrated to reach a steady state after about 10 ms.

3) Regular and Irregular neurons: the term $\sigma\xi(t)$ in eqn. (3) is used to distinguish regular and irregular neurons. Indeed by using different sigma in the Gaussian noise term we were able to obtain a clear distinction in between regular and irregular afferent neurons. In our hardware we achieved distinction by externally stimulating irregular neurons via two fixed synapses (one excitatory and one inhibitory) with two distinct Gaussian spike trains of $\mu = 180$ Hz and $\sigma = 0.2$. Fig. 2 shows the result of this calibration.

In Fig. 2c and Fig. 2d we show the Power Spectral Density (PSD) of neuron's spontaneous activity for regular and irregular conditions. In the regular condition the neuron shows low variability in its Inter Spike Interval. This is reflected in the PSD of Fig. 2c, which contains peaks at the resting state ($\sim$ 100 Hz) as well as integer multiples representing higher harmonics. On the other hand, the neuron's response in the irregular condition showed a much less structured PSD with only a clear peak at his fundamental frequency ($\sim$ 100 Hz, mean rate spiking frequency).

The coefficient of variation (CV*) is computed as the normalized ratio between the SD and the mean of the ISI distribution [2]. The variability at resting state is a good indicator of the DC component and explains the difference of the two spectral densities at low frequencies. See Fig. 2c and Fig. 2d.

III. Results

CV results and plots in Fig. 2 show that the resting discharges of the regular and irregular neurons are compatible with the biological data from [1]. In terms of coefficient of

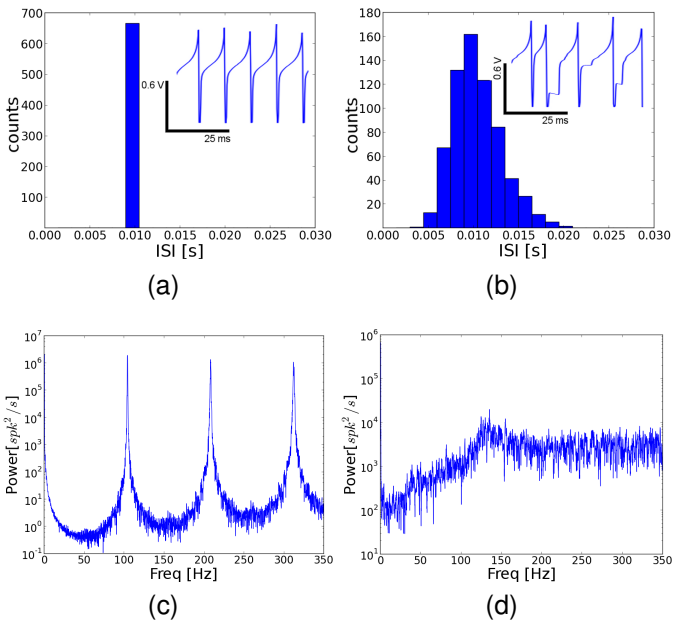

Fig. 2. **Measured membrane potentials, Inter-Spike Interval (ISI) distributions, and power spectra density analysis** (a) Regular neuron ISI histogram at resting (spontaneous activity condition). The inset shows a snapshot of the membrane potential recorded from the chip. (b) neuron ISI for the irregular spontaneous activity condition at rest. Sub-figures: (c), (d) shows the PSD for regular and irregular neurons. Note that the regular neuron has three peaks in the PSD. In contrast, irregular neuron shows an higher energy distribution in low frequency.

variation a neuron is classified regular for $CV^* < 0.15$ and irregular otherwise. We obtained a $CV^*_{reg} = 0.0022$, $CV^*_{irr} = 0.4541$. Moreover, from the power spectrum it is possible to deduce the amount of noise at each frequency component during resting state. To obtain better information transmission one must increase the Signal-To-Noise ratio (SNR). Therefore lower noise at specific frequency ranges will give rise to higher SNR. The lower PSD for regular neurons supports a better coding of lower head velocities, thus our results are compatible with the biological reference [1].

Dissimilar shape for the PSD supports the hypothesis that regular and irregular neurons code differently the frequency information. Noise in the irregular neurons plays an important functional role in flattening the PSD and in turn it affects the information encoding.

The tuning of silicon neurons showed good linearity in the spiking response over the frequency range 300 - 1500 Hz (Fig. 3). As shown in Fig. 4, properly conditioning the gyro's output data has led the exponential LIF silicon neuron to act as an afferent for an artificial neuromorphic vestibular system. In particular, high correlation coefficient values have been obtained, both for the regular and irregular afferents, between output spiking rate and the input velocity form the gyro (respectively $R_{reg} = 0.65$ and $R_{irreg} = 0.73$).

IV. Conclusions

In this work we developed an artificial neuromorphic vestibular sensor, using a commercial IMU and a neuromor-

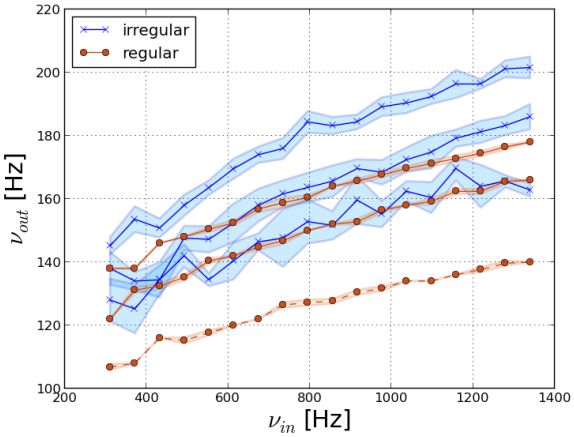

Fig. 3. **Input/output characteristic of the vestibular afferents:** Firing rate as a function of PDM for 6 neurons: regular (circles) and irregular (crosses). Shaded areas represent the standard deviation of four different stimulations.

phic CMOS VLSI chips comprising adaptive integrate and fire neurons and synapses with biologically plausible temporal dynamics. We calibrated the chip to match the parameters of a neuroscientific computational model and the presented experimental results validate the hardware implementation and the calibration procedure. The same PSDs for both regular and irregular afferents have been reproduced and we obtained an almost linear characteristic of the input/output response.

The constraints imposed on the implementation by the architecture of the sensor's processing unit have been met with respect to the required timing stability of the output PDM signal (Fig. 4). In order to accurately drive the output to the chip, higher priority has been given to the PDM timer interrupt, a lower one to the data acquisition. The impact of this choice on the reconstructed signal could be further investigated in terms of the latency introduced in the system's response to angular velocity variations, especially at high speed, when the firing rate is maximum.

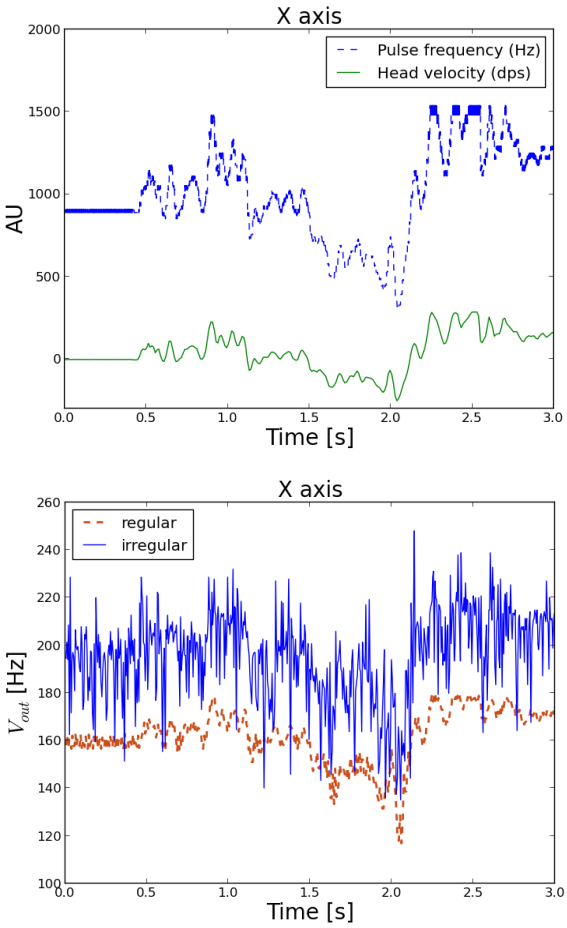

Fig. 4. **Vestibular system input and output:** up) The output signal of the IMU unit (both angular velocity and associated PDM frequency). down) The corresponding neuron's mean firing rates in response to those inputs. Analogous plots have been measured for the Y and Z axes (not shown).

Acknowledgments

The authors would like to thank Italian Ministry of Foreign Affairs, General Directorate for Cultural Promotion and Cooperation, for its support to the establishment of the Robot-An joint laboratory, and the "neuroP" Project, ERC-2010-StG-257219-neuroP.

References

[1] S. G. Sadeghi, M. J. Chacron, M. C. Taylor, and K. E. Cullen, "Neural variability, detection thresholds, and information transmission in the vestibular system," *The Journal of Neuroscience*, vol. 27, no. 4, pp. 771–781, Jan. 2007.

[2] J. M. Goldberg, C. E. Smith, and C. Fernández, "Relation between discharge regularity and responses to externally applied galvanic currents in vestibular nerve afferents of the squirrel monkey," *Journal of neurophysiology*, vol. 51, no. 6, pp. 1236–1256, June 1984.

[3] A. Berthoz, *The Brain's Sense of Movement (Perspectives in Cognitive Neuroscience)*. Harvard University Press, Sept. 2002.

[4] T. Constandinou, J. Georgiou, and C. Toumazou, "Towards an integrated, fully-implantable vestibular prosthesis for balance restoration," *Advances in Science and Technology*, vol. 57, pp. 210–215, 2008.

[5] P. Dario, M. C. Carrozza, E. Guglielmelli, C. Laschi, A. Menciassi, S. Micera, and F. Vecchi, "Robotics as a future and emerging technology biomimetics, cybernetics, and neuro-robotics in european projects," *IEEE Robotics & Automation Magazine*, vol. 12, no. 2, pp. 29–45, June 2005.

[6] S. G. Sadeghi, L. B. Minor, and K. E. Cullen, "Response of vestibular-nerve afferents to active and passive rotations under normal conditions and after unilateral labyrinthectomy," *Journal of neurophysiology*, vol. 97, no. 2, pp. 1503–1514, Nov. 2006.

[7] K. A. Boahen, "Point-to-point connectivity between neuromorphic chips using address-events," *IEEE Transactions on Circuits and Systems II*, vol. 47, no. 5, pp. 416–434, May 2000.

[8] R. Brette and W. Gerstner, "Adaptive exponential integrate-and-fire model as an effective description of neuronal activity," *Journal of neurophysiology*, vol. 94, no. 5, pp. 3637–3642, 2005.

[9] S. Moradi and G. Indiveri, "An event-based neural network architecture with an asynchronous programmable synaptic memory," *IEEE Transactions on Biomedical Circuits and Systems*, March 2013.

[10] G. Indiveri, B. Linares-Barranco, T. J. Hamilton, A. van Schaik, R. Etienne-Cummings, T. Delbruck, S.-C. Liu, P. Dudek, P. Häfliger, S. Renaud, J. Schemmel, G. Cauwenberghs, J. Arthur, K. Hynna, F. Folowosele, S. Saighi, T. Serrano-Gotarredona, J. Wijekoon, Y. Wang, and K. Boahen, "Neuromorphic silicon neuron circuits," *Frontiers in Neuroscience*, vol. 5, no. 73, May 2011.